Formation of Lanthanide (III) Cubanes to Dimer Assemblies- coordination geometry influence on structure, single-molecule magnetism and photoluminescence

Ho-Yin Wong, Wesley Ting Kwok Chan, Ga-Lai Law*

Department of Applied Biology and Chemical Technology, the Hong Kong Polytechnic University, Hung Hom, Hong Kong

ABSTRACT. Although the hydrolytic synthesis of lanthanide(III) clusters is well-established, it is scarcely studied along the whole Ln^{III} series. In this work, tetranuclear cubane-like clusters, $Ln_4(\mu_3\text{-}OH)_4(\mu\text{-}tfa)_4(hfa)_4(phen)_4$ (**1–9**, Ln = La–Dy (except Pm), tfa = trifluoroacetate, hfa = hexafluoroacetylacetonate), and dinuclear clusters, $Ln_2(\mu\text{-}OH)_2(hfa)_4(phen)_2$ (**10–16**, Ln = Tb–Lu), were synthesized and characterized, demonstrating that the size of the Ln^{III} ions determines the type of clusters formed due to preferential differences in the formation of the coordination geometry. Evaluation of these topological assemblies shows unusual magnetic and optical properties, for example, cubane-like Dy_4 single molecule magnet (SMM) is rare. In our work, we show that **8**-Tb_4 and **9**-Dy_4 are ferromagnetically coupled and display unexpectedly good SMM behavior. The anisotropic barrier of the Dy^{III} compound, U_{eff}, was measured at 67.0 K under a zero-dc magnetic field. As expected for dinuclear compounds, **11**-Dy_2 possesses intramolecular antiferromagnetic interactions and behaves as an SMM with U_{eff} of 82.5 K. In addition, the solid-state photoluminescence study showed that **6**-Eu_4 and **8**-Tb_4 are emissive at room temperature and their photophysical properties are discussed.

INTRODUCTION

The exploration of polynuclear lanthanide(III) compounds is a highly active and important area of research over the last two decades due to its importance in many aspects of applications, such as optical, magnetic and catalytic applications. The oxo/hydroxo clusters are one of the important classes of such compounds.[1] The selection of appropriate shielding ligands to stabilize the cluster core and prevent polymerization is the key to the rational design and synthesis of these compounds.[2] The most commonly employed ligands are β-diketones such as dibenzylmethane[3] and acetylacetone[4] which allow the formation of clusters with different nuclearities by controlling the reaction conditions.[5] The tetranuclear cubane-like core, which is well-documented among

transition metal and lanthanide(III) ions, is one example. According to the Cambridge Structural Database (CSD), there are around 2019 entries of transition metal hydroxo-cubane-like clusters but there are only 202 of the Ln^{III} counterpart.[6] The scarce examples of lanthanide assemblies reported in literature is due to the difficulty in controlling the desiredtopological formations due to the variable range of coordination numbers possible with the lanthanides.[7] Although challenging, such compounds are still worth investigating due to their intriguing physical properties such as molecular magnetism and photoluminescence.

Single-molecule magnets (SMMs) are discrete molecules that retain magnetization upon removal of an external magnetic field at low temperature.[8] The large magnetic anisotropy of Ln^{III} ions often leads to the slow relaxation of magnetization of their complexes. The search of molecules with large anisotropic barrier, U_{eff}, and blocking temperature, T_B, is crucial for developing memory-based molecular devices. The highest U_{eff} and T_B reported to date are 1815 K and 60 K respectively for Dy^{III}-based single-ion magnets (SIMs).[9,10] However, these examples involves single metal ions and therefore cannot be correlated to polynuclear Ln^{III} SMMs structures where the mechanism is different. This affords an independent and important area of study into polynuclear assemblies such as cubane, as it provides insight into the complicated magnetic mechanism arising from multi-metal centers which exhibit unique features such as multiple relaxation processes.[11] To circumvent the difficulty in obtaining a large ground spin state, choosing appropriate ligands for the formation geometry is important. It has been shown that the tuning of the anisotropic barrier is achievable, with 530 K being the highest record for a Dy_5 pyramid.[12] However, only a few examples of Ln^{III} cubane-like tetranuclear cluster SMM are reported and these are often weak because of fast quantum tunneling of magnetization (QTM).[13] Here we give a new example of a Dy cubane that has a sizable SMM property.

Furthermore, luminescent lanthanide(III) complexes are useful in the development of optical devices.[14] Due to the parity-forbidden 4f–4f transition of Ln^{III} ions, their luminescence is often achieved by the antenna effect, i.e. the excitation of ligands, followed by the transfer of excited energy to the Ln^{III} ions to stimulate metal-centered luminescence.[15] In general, the triplet state of the ligands lying 2500–3500 cm^{-1} above the excited state of the Ln^{III} ions would lead to efficient energy transfer.[16] β-Diketonates are known to be efficient sensitizers for Eu^{III} and sometimes, Tb^{III} ions.[17] Their hydroxo clusters also display decent luminescent properties.[18]

While examples of hexafluoroacetylacetonate (hfa) clusters in literature are mostly dinuclear, for their tetranuclear cubane-like counterpart, only $[Gd_4(\mu_3\text{-}OH)(\mu\text{-}H_2O)_2(H_2O)_4(hfa)_8]\cdot2C_6H_6\cdot H_2O$ has been reported.[19] In regard of this, hfa-based clusters were synthesized throughout the Ln^{III} series (except Pm^{III}), and trifluoroacetate (tfa) and 1,10-phenanthroline (phen) served as co-ligands to provide extra shielding from polymerization, resulting in cubane-like clusters **1-9** and dinuclear compounds **10-16** (Figure 1). Two Ln_4 cubanes, **8**-Tb_4 and **9**-Dy_4, showed slow relaxation of magnetization with the U_{eff} greater than most of the Dy^{III} monocubane for the Dy_4. The magnetic property of **11**-Dy_2 from the dimer series are also included for comparison purpose in this work. The solid-state photophysical properties of the visible emitters, **6**-Eu_4, **8**-Tb_4 and **10**-Tb_2 are also reported as well.
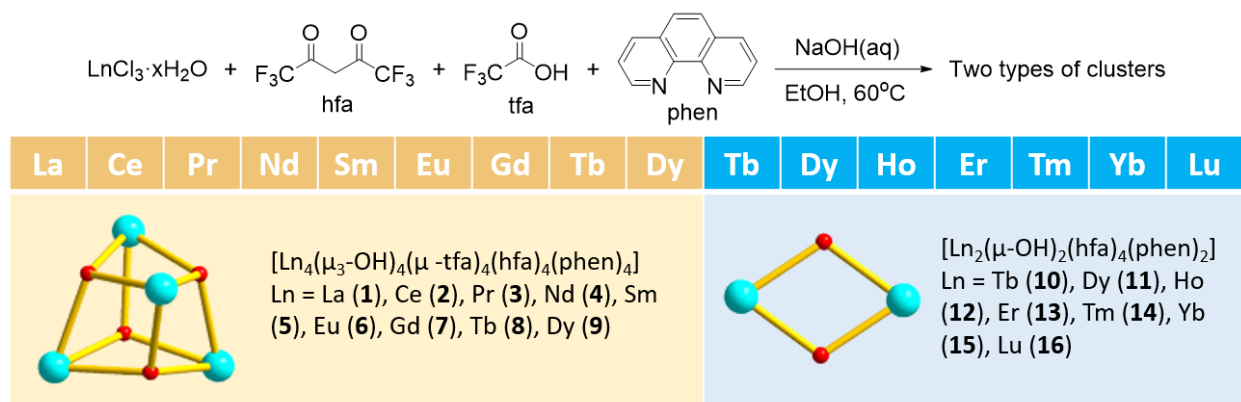
Figure 1. The synthetic route of the clusters: cubane (left); dimer (right). Colour code: Ln (blue), O (red). When Ln = La and Ce, x = 7; when Ln = Pr–Lu, x = 8.

RESULT AND DISCUSSION

Synthesis and characterization. Two types of clusters, $Ln_4(\mu_3\text{-OH})_4(\mu\text{-tfa})_4(hfa)_4(phen)_4$ and $Ln_2(\mu\text{-OH})_2(hfa)_4(phen)_2$, were obtained by the reaction in Figure 1, in which a precipitate was rapidly formed and purified by recrystallization with a mixture of acetone and ethanol. At the beginning of this study, compounds **1–7** and **10–16** were obtained through the reaction of lanthanide(III) salt, hfa, phen and NaOH in the ratio of 1:3:1:3. Single crystal structure analysis affirmed that **1–7** are tetranuclear cubane-like clusters and **10–16** are dinuclear complexes (see the section on Crystal structures). The formation of the cluster can be explained by the theory of "ligand-controlled hydrolytic approach".[5] Since Ln^{III} ions are Lewis acids in nature, under high pH, hydrolysis is triggered and Ln–OH units are formed. Next, olation would occur, i.e. one OH ligand would participate in bridging interactions with additional Ln^{III} ions. Organic ligands (hfa, tfa and phen) chelate Ln^{III} ions for controlling the olation process, resulting in desirable structures. In this case, $[Ln_4(\mu_3\text{-OH})_4]^{8+}$ and $[Ln_2(\mu\text{-OH})_2]^{4+}$ cores were generated. The formation of tfa is likely to be due to the hydrolysis of hfa.[20] In an attempt to obtain the tetranuclear clusters of Tb^{III}

5

to Lu^{III}, tfa was introduced to the synthesis. Surprisingly, **8**-Tb$_4$ and **9**-Dy$_4$ were isolated but not for the series of Ho^{III} to Lu^{III}. Since the ionic radii of Ho^{III} to Lu^{III} are smaller, their sizes may not favour the formation of our type of Ln$_4$ cluster.[2] Hence, the attempt to synthesize the tetranuclear clusters for the latter Ln^{III} series, even by adding more equivalence of base or switching to different bases, such as organic bases, like trimethylamine failed.

The complexes were characterized by CHN elemental analysis and FT-IR spectroscopy (Figures S1–16). For **1**-La$_4$, **5**-Sm$_4$ and **6**-Eu$_4$, ^{1}H NMR was also employed for additional characterization (Figures S17–19). The FT-IR spectra of the cubane and dimer are similar due to the C=O and C–F bonds; however, the absorption peaks attributed to the stretching of the bridging OH bonds allow the differentiation of these two types of clusters.[21] The tetranuclear clusters show a sharp peak at around 3600 cm^{-1} while that of dinuclear compounds is at around 3700 cm^{-1}, as shown from the Tb^{III} and Dy^{III} compounds (Figure 2). The lower wavenumber of **8**-Tb$_4$ and **9**-Dy$_4$ is attributed to the μ_3 binding mode which weakened the O–H bonds more than the μ_2 mode of **10**-Tb$_2$ and **11**-Dy$_2$.
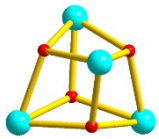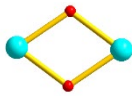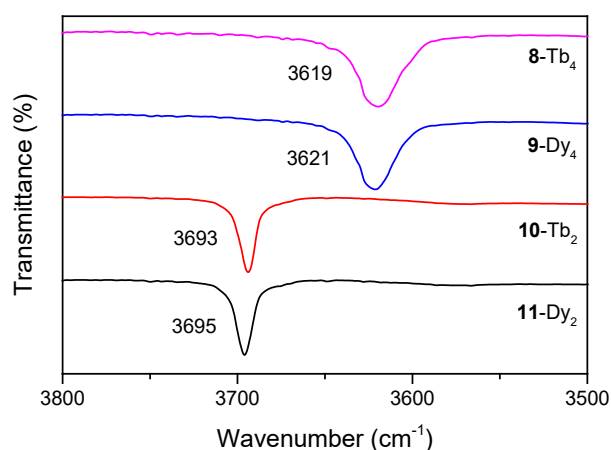

Figure 2. The FT-IR spectra of compounds **8**–**11** in the range of 3500 to 3800 cm^{-1}.

Table 1. The bond lengths and angles within the cluster cores of compounds **1**–**16**.

Cluster cores[a]	Compounds	Ln–OH (Å)[b]	Ln–O–Ln (°)[b]	O–Ln–O (°)[b]	Ln…Ln distance (Å)[b]
	1-La$_4$	2.515 ± 0.010	108.34 ± 3.86	67.45 ± 2.01	4.076 ± 0.089
	2-Ce$_4$	2.500 ± 0.022	108.07 ± 3.30	67.93 ± 1.78	4.045 ± 0.064
	3-Pr$_4$	2.482 ± 0.022	108.13 ± 3.26	67.86 ± 1.75	4.017 ± 0.068
	4-Nd$_4$	2.466 ± 0.019	108.15 ± 3.10	67.85 ± 1.64	3.992 ± 0.066
	5-Sm$_4$	2.438 ± 0.025	108.00 ± 2.40	68.15 ± 1.30	3.945 ± 0.042
	6-Eu$_4$	2.422 ± 0.019	107.97 ± 2.22	68.22 ± 1.15	3.919 ± 0.041
	7-Gd$_4$	2.419 ± 0.012	107.78 ± 2.15	68.52 ± 1.09	3.906 ± 0.043
	8-Tb$_4$	2.405 ± 0.015	107.78 ± 2.10	68.50 ± 1.08	3.886 ± 0.041
	9-Dy$_4$	2.393 ± 0.020	107.83 ± 2.21	68.42 ± 1.72	3.867 ± 0.039
	10-Tb$_2$	2.257 ± 0.009	109.68	70.32	3.690
	11-Dy$_2$	2.239 ± 0.014	110.10	69.90	3.668
	12-Ho$_2$	2.237 ± 0.085	109.50	70.50	3.655
	13-Er$_2$	2.221 ± 0.065	109.87	70.13	3.636
	14-Tm$_2$	2.210 ± 0.045	110.00	70.00	3.623
	15-Yb$_2$	2.201 ± 0.011	109.77	70.23	3.601
	16-Lu$_2$	2.194 ± 0.010	109.98	70.02	3.594

[a] Colour code: Ln (blue), O (red). [b] Average values within the cluster cores.

Crystal structures. All single crystals were obtained by slow evaporation of an acetone/ethanol mixture. Single crystal structure analysis by X-ray revealed that the Ln$_4$ clusters are isostructural but not isomorphous in terms of space group since **1**–**5** are $I4_1/a$ and **6**–**9** are $Pbcn$ (Table S1). These clusters all possess a cubane-like tetranuclear core (**1**-La$_4$ in Figure 3). Each Ln^{III} ion is nine-coordinated by three μ_3-OH groups, one hfa, one μ-tfa and one phen. The bond lengths and angles of the cluster cores are summarized in Table 1. The deviation of the bond angles from 90° indicates a distorted cubane core. In general, Ln–OH bond lengths and Ln…Ln interactions decrease along the series due to lanthanide contraction while Ln–O–Ln and O–Ln–O bond angles remain almost unchanged. The asymmetric unit is one-fourth of the cluster for **1**–**5** and half for **6**–**9**. Since the **5**-Sm$_4$ crystal is air-sensitive (but the bulk compound is not as demonstrated by FT-IR and NMR spectra), the X-ray diffraction data was collected at 150 K; as such, acetone molecules are present in the lattice. Aside from **5**-Sm$_4$ and **6**-Eu$_4$, acetone molecules are absent, leaving a solvent-accessible void of around 260 Å^3 (Figure S20). To further investigate this feature, data of the **2**-Ce$_4$ crystal were collected at 150 K right after leaving the mother liquid. As expected, acetone

molecules were found. When the temperature was raised to room temperature, it was observed that, the acetone molecules vanished and a cavity was formed again (Figure S20), indicating that the 3D structures were strongly maintained by the intermolecular and intramolecular π-interactions at room temperature (Figure S21).
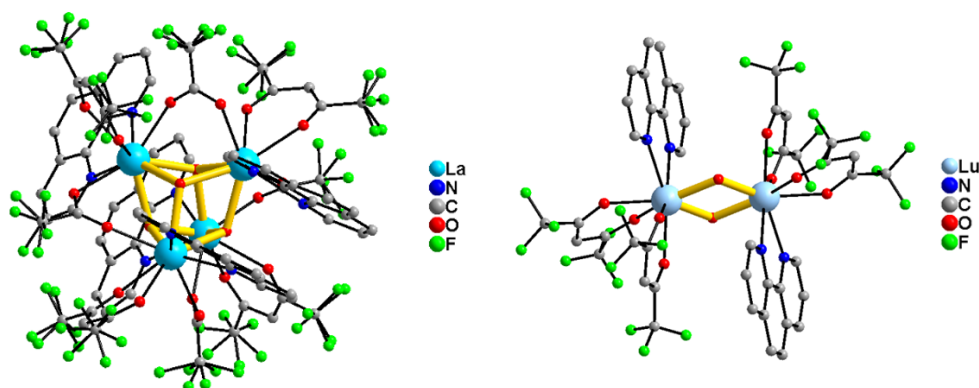

Figure 3. The crystal structures of **1**-La$_4$ and 16-**Lu**. The cores are in yellow. Hydrogen atoms are omitted for clarity.

In contrast, the Ln$_2$ clusters **10-16** are isostructural with the same space group of P-1 (Table S1). Each Ln^{III} ion is eight-coordinated and surrounded by two μ-OH groups, two hfa and one phen (**16**-Lu$_2$ in Figure 3). By comparing the structures of **10**-Tb$_2$ and **11**-Dy$_2$ with those of **8**-Tb$_4$ and **9**-Dy$_4$, while the Ln–O–Ln and O–Ln–O angles remain almost unchanged, the Ln–OH bonds and Ln…Ln distances of Ln$_2$ are shorter, showing resistance to elongation to form the cubane-like core.

Aside from **8**-Tb$_4$ and **9**-Dy$_4$, the synthetic procedures are the same for the rest of the compounds. The change from cubane to dimer is likely to be due to lanthanide contraction. Literature examples are rarely available for such structural rearragement.[22] For example, Zheng's group established a series of Ln^{III} hydroxo clusters using acetylacetone as a chelator. For La^{III} and Pr^{III}, nine-

coordinated polymeric complexes were favourable whereas for the heavier Ln^{III}, eight-coordinated cubane-like or nonanuclear clusters were assembled instead. To gain more insight into the trend, the coordination geometries of the clusters were determined by using the shape analysis program developed by Raymond's group (Table S2).[23] Interestingly, for the cubane-like cluster, **1**–**5** are closer to an idealized tricapped trigonal prism (D_{3h}) while **6**–**9** are more likely to be capped square antiprism (C_{4v}) (Figure S22). For the Ln_2 clusters, **10**-Tb_2, **11**-Dy_2 and **12**–**16** resemble trigonal dodecahedron (D_{2d}), bicapped trigonal prism (C_{2v}) and square antiprism (D_{4d}), respectively (Figure S22). Note that these are all distorted geometry which is an intermediate between one and other. Interestingly, the geometries **10**-Tb_2 and **11**-Dy_2 deviate from the dimer series and they can form the cubane-like **8**-Tb_4 and **9**-Dy_4. The intermolecular interactions may cause structural discrepancy (Figure S21). For compounds **1**–**5**, a 3D network is bridged by intermolecular π-interactions of phen rings in a parallel-displaced fashion under which the voids are tolerated. For **6**–**9**, the whole structures are no longer supported by the intermolecular π-interactions. In contrast, **10**–**16** bear an extensive phen ring stacking to build a 1D chain. Such a stable system is more preferred than the **6**–**9** cubane structure.

Magnetic properties. The magnetic properties of compounds **7**–**12** were investigated. Temperature-dependent magnetic direct current (dc) susceptibility measurements were performed under 1000 Oe applied field between 300 to 2 K. The plots of $\chi_M T$ vs T are displayed in Figure 4, where χ_M is the molar magnetic susceptibility. At 300 K, the $\chi_M T$ values of **7**–**12** are 29.8, 44.0, 54.6, 22.9, 24.0 and 26.2 cm^3 mol^{-1} K respectively. The theoretical values of four magnetically isolated Gd^{III} ($^8S_{7/2}$, $g = 2$), Tb^{III} ($^7F_6$, $g = 3/2$) and Dy^{III} ($^6H_{15/2}$, $g = 4/3$) are 31.5, 47.3 and 56.7 cm^3 mol^{-1} K, and those of two uncoupled Tb^{III}, Dy^{III} and Ho^{III} ($^5I_8$, $g = 5/4$) are 23.6, 28.3 and 29.0 cm^3 mol^{-1} K, respectively. The experimental values are slightly smaller than but close to the

expected ones. The $\chi_M T$ values of **7**-Gd$_4$ and **10**-Tb$_2$ remain almost constant within the temperature range of 300-50 K, they then decrease to a minimum of 18.6 and 9.0 cm^3 mol^{-1} K at 2 K. This phenomenon is due to a progressive depopulation of excited Stark sublevels or the weak antiferromagnetic interactions between the Ln^{III} ions.[24] A more detailed analysis of **7**-Gd$_4$ using the spin-Hamiltonian $H = 2J_{ex}(S_{Gd1}\cdot S_{Gd2} + S_{Gd1}\cdot S_{Gd3} + S_{Gd1}\cdot S_{Gd4} + S_{Gd2}\cdot S_{Gd3} + S_{Gd2}\cdot S_{Gd4} + S_{Gd3}\cdot S_{Gd4})$ where $S_{Gd1} = S_{Gd2} = S_{Gd3} = S_{Gd4} = 7/2$ and J_{ex} is the exchange constant, afforded the best fit curve with J_{ex} = -0.052 cm^{-1} and g = 1.95, confirming the antiferromagnetic nature.[25] In contrast, for **8**-Tb$_4$, **9**-Dy$_4$, **11**-Dy$_2$ and **12**-Ho$_2$, the $\chi_M T$ value decreases gradually upon cooling, and increases at lower temperatures until 2 K. This behavior is due to the presence of intramolecular weak ferromagnetic interactions within the complexes, which are strong enough to overcome the crystal field effects.[25,26]
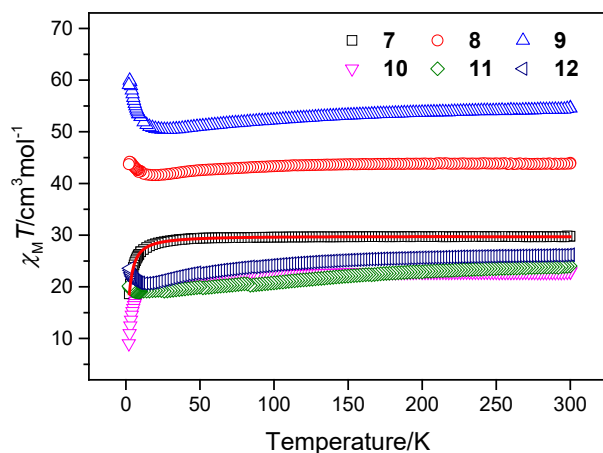

Figure 4. Temperature-dependence of magnetic susceptibilities, $\chi_M T$ *vs. T*, for **7**–**12** at 1000 Oe. The red solid line of **7**-Gd$_4$ corresponds to the best fit curve.

The measurement of the dynamic magnetic properties of compounds **8**–**11** was carried out in a zero-dc field. Due to the large magnetic anisotropy of Tb^{III} and Dy^{III} ions, the temperature and

frequency dependences of the in-phase (χ_M') and out-of-phase (χ_M'') alternating current (ac) susceptibility displayed a slow relaxation of the magnetization and suggested an SMM nature of **11**-Dy$_2$, and surprisingly **8**-Tb$_4$ and **9**-Dy$_4$, since cubane-like Ln^{III} SMMs are rarely known or very weak.[27] Furthermore, peak maxima exist in the out-of-phase plots of **9**-Dy$_4$ and **11**-Dy$_2$ (Figure 5 and S23); thus extra insight into the relaxation dynamics can be gained by plotting ln τ versus $1/T$, where τ is the relaxation time (Figure 6). The curvature of the plots indicates multiple relaxation processes and these two SMMs display different properties. At the high-temperature regime, both compounds show linear dependence of ln τ on $1/T$, suggesting relaxation *via* Orbach mechanism. However, for **11**-Dy$_2$, ln τ become independent of $1/T$ at lower temperature where the quantum regime begins, while for **9**-Dy$_4$, a weak temperature dependency can still be observed, indicating the Raman relaxation process. The data is fitted with the equation $\tau^{-1} = \tau_0^{-1}\exp(-U_{eff}/k_BT) + CT^n + \tau_{QTM}^{-1}$ to consider the Orbach and Raman relaxation processes and QTM,[28] affording U_{eff} = 67.0 K and τ_0 = 1.22 x 10^{-8} s for **9**-Dy$_4$, and U_{eff} = 82.5 K and τ_0 = 1.73 x 10^{-7} s for **11**-Dy$_2$, where U_{eff} is the anisotropic barrier and τ_0 is the attempt time. The fitting parameters are displayed in Table S5. The molar susceptibility measurement was also conducted in an optimized dc field of 2000 Oe (Figure S24–S25) to reduce QTM. The same calculation conferred U_{eff} = 78.6 K and τ_0 = 1.3 x 10^{-8} s for **9**-Dy$_4$ and U_{eff} = 86.1 K and τ_0 = 1.3 x 10^{-8} s for **11**-Dy$_2$ (Figure S26 and Table S5), which do not deviate much from the zero-field values. Cole-Cole diagrams of **9**-Dy$_4$ and **11**-Dy$_2$ were constructed to resolve the distribution of the relaxation time. In Figure 7, the plots show a general arc formation in the temperature range of 2–7 K, which can be fitted using the generalized Debye model.[29] The afforded α parameter is in the range of 0.09 to 0.18 for **9**-Dy$_4$ and 0.13 to 0.27 for **11**-Dy$_4$, indicative of a narrow width of distribution in the single relaxation process for both compounds (Table S3–S4). Although the ac measurement demonstrated the SMM behaviour of **8**-

Tb4, **9**-Dy4 and **11**-Dy2, no hysteresis loops were observed in the magnetic study at 2 K (Figure S27).
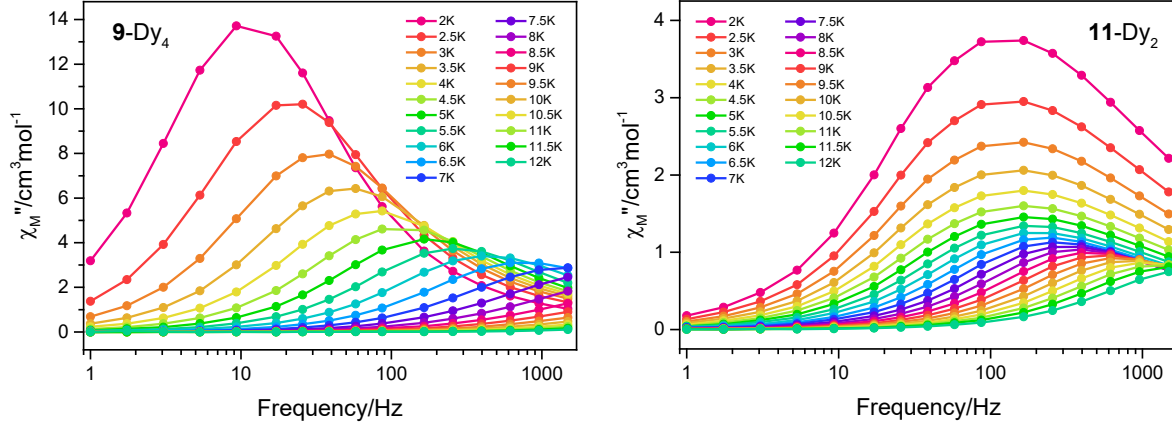

Figure 5. Frequency dependence of the out-of-phase ac susceptibility under zero-dc field of **9**-Dy4 and **11**-Dy2. The solid lines are the visual guides.
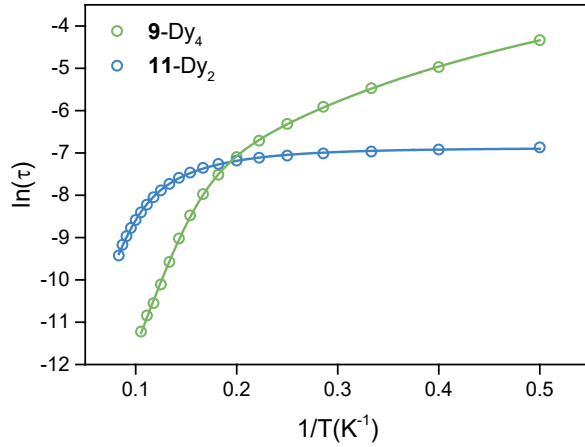

Figure 6. Arrhenius plots of relaxation time data for **9**-Dy4 and **11**-Dy2. The solid lines correspond to fits to the equation $\tau^{-1} = \tau_0^{-1}\exp(-U_{eff}/k_BT) + CT^n + \tau_{QTM}^{-1}$.
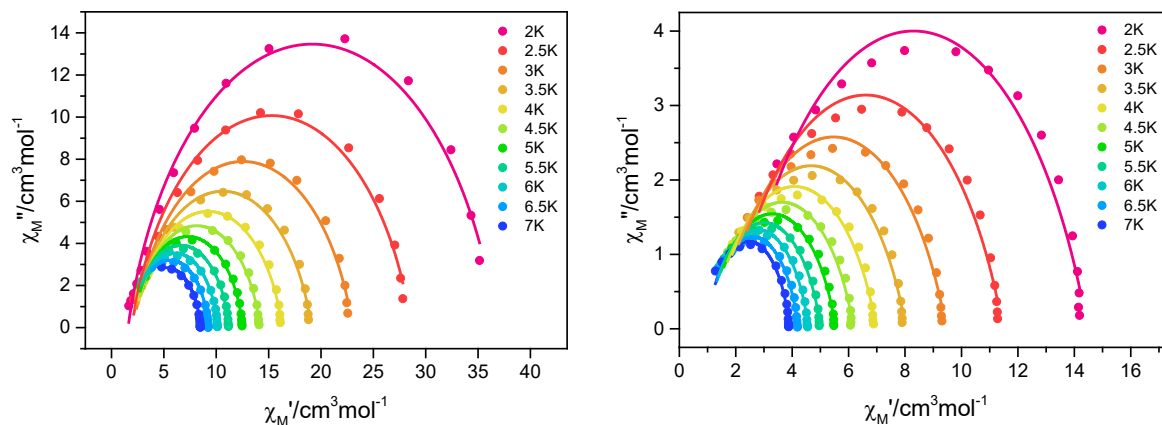
Figure 7. The Cole-Cole plots for **9**-Dy$_4$ (left) and **11**-Dy$_2$ (right) obtained using the ac susceptibility data. The solid lines correspond to the best fits obtained with a generalized Debye model.[29]

To correlate the magnetic and structural properties in SMM Dy^{III} cubane-like clusters, a summary of bond lengths and angles and intramolecular Dy…Dy distances of **9**-Dy$_4$ and some literature examples were included in Table 2. Ke *et al.* proposed that Dy^{III} cubanes are likely to display SMM behavior, if their Dy–O–Dy angles are greater than 99°.[27f] **9**-Dy$_4$ are found to be in the range of 105.15^o to 110.80^o with an average of 107.8 $\pm$ 2.2^o, which is in general larger compared to other cubanes and further supports this hypothesis. Apart from that, the average Dy…Dy distance of **9**-Dy$_4$, 3.87 $\pm$ 0.04 Å, is the largest due to the longer Dy–OH bonds, larger Dy–O–Dy and smaller O–Dy–O angles which pull the Dy^{III} ions apart. This slight structural difference may alter the magnetic interaction,[27f] leading to the weak ferromagnetic interaction within **9**-Dy$_4$. Another example is [Dy$_4$(OH)$_4$(SO$_4$)$_3$(ox)(H$_2$O)$_6$], which has comparable Dy–O–Dy and O–Dy–O angles.[27g] Although ferromagnetically coupled, its SMM was not reported, which may be due to the shorter Dy…Dy intramolecular distance. It is noticeable that when this average distance is

13

smaller than 3.85 Å, either weak SMM or non-SMM results. This is likely to be due to a stronger exchange interaction within the cubane core.

Table 2. Comparison of magnetic properties of some Ln^{III} cubane-like clusters.

Compounds	Dy–OH (Å)[a]	Dy–O–Dy (°)[a]	O–Dy–O (°)[a]	Dy...Dy distance (Å)[a]	SMM[b]	U_{eff} (K)[c]	Ref
9-Dy$_4$ [Ln$_4$(μ_3-OH)$_4$(μ-tfa)$_4$(hfa)$_4$(phen)$_4$]	2.393 ± 0.020	107.8 ± 2.2	68.4 ± 1.2	3.867 ± 0.039	Yes	67.0	This work
[Dy$_4$(L)$_4$(μ_2-$\eta_1\eta_1$Piv)$_4$]·4H$_2$O·6CH$_3$OH	2.440 ± 0.054[d]	104.7 ± 6.8	71.7 ± 4.3	3.858 ± 0.216	Yes	43.4	27a
[Dy$_4$(μ_3-OH)$_4$(Acc)$_6$(H$_2$O)$_7$(ClO$_4$)]·(ClO$_4$)$_7$·11H$_2$O	2.369 ± 0.049	106.5 ± 2.4	70.4 ± 1.2	3.795 ± 0.035	Yes	-	27b
[Dy$_4$(μ_3-OH)$_2$(μ_3-O)$_2$(cpt)$_6$(MeOH)$_6$(H$_2$O)]$_2$	2.37 ± 0.03	106.1 ± 1.6	71.1 ± 0.9	3.784 ± 0.033	Yes	-	27c
[Dy$_4$(μ_3-OH)$_4$(nic)$_6$(py)(MeOH)$_7$][ClO$_4$]$_2$·py·4CH$_3$OH	2.359 ± 0.029	106.4 ± 2.0	70.6 ± 1.3	3.776 ± 0.048	Yes	-	27d
[Dy$_4$(μ_3-OH)$_3$(μ_3-O)(NOPyCOO)$_6$(OH)(H$_2$O)$_3$·(DMF)$_3$(H$_2$O)$_{12}$]$_\infty$	2.351 ± 0.040	106.2 ± 1.6	70.5 ± 1.1	3.755 ± 0.006	Yes	-	27e
Dy$_8$(HL)$_{10}$(C$_6$H$_4$NH$_2$COO)$_2$(μ_3-OH)$_8$(OH)$_2$(NO$_3$)$_2$(H$_2$O)$_4$	2.36 ± 0.026	106.2 ± 2.0	70.8 ± 1.2	3.769 ± 0.057	Yes	-	27f
[Dy$_4$(HL)$_4$(C$_6$H$_4$NH$_2$COO)$_2$(μ_3-OH)$_4$(μ-OH)$_2$(H$_2$O)$_4$]$_3$·4CH$_3$CN$_3$·12H$_2$O	2.355 ± 0.012	105.7 ± 4.8	71.2 ± 2.4	3.751 ± 0.114	No	-	27f
[Dy$_4$(OH)$_4$(SO$_4$)$_3$(ox)(H$_2$O)$_6$]	2.380 ± 0.040	107.0 ± 1.7	69.9 ± 0.8	3.823 ± 0.039	-	-	27g
[Dy$_4$(OH)$_4$(SO$_4$)$_4$(H$_2$O)$_3$]	2.356 ± 0.054	107.5 ± 2.6	68.9 ± 1.9	3.799 ± 0.045	-	-	27g
{[Dy$_4$(OH)$_4$(asp)$_3$(H$_2$O)$_8$](ClO$_4$)$_2$·10H$_2$O}$_n$	2.357 ± 0.033	106.61 ± 1.92	70.27 ± 1.46	3.779 ± 0.044	-	-	27h
(H$_3$O)$_4$[Dy$_4$(OH)$_5$(H$_2$O)$_4$(μ_2-IN)(IN@CB[6])$_2$]Br	2.352 ± 0.028	106.6 ± 3.2	70.2 ± 2.2	3.769 ± 0.080	-	-	27i
[Dy$_4$(OH)$_8$(H$_2$O)$_3$(IN@CB[6])$_2${Ag(H$_2$O)$_2$(HIN)}{Ag(H$_2$O)$_2$-(IN)}][Ag(H$_2$O)$_2$(CB[6])](NO$_3$)$_4$·28H$_2$O	2.348 ± 0.042	106.0 ± 3.4	71.1 ± 2.0	3.748 ± 0.079	-	-	27i
[Dy$_4$(μ_3-OH)$_4$(nmc)$_8$]	2.360 ± 0.049	104.8 ± 4.6	72.3 ± 2.8	3.737 ± 0.109	-	-	27j

[a] Average values of the cluster core. [b] SMM positive if it displays any out-of-phase ac susceptibility signal. Blank entries mean no dynamic magnetic properties were reported [c] Blank entries indicate no peak maxima can be found in the out-of-phase ac susceptibility plot. [d] Ln-O$_{alkoxy}$ bond length.

Photoluminescent properties. Solid-state photoluminescence study at room temperature was performed and only **6**-Eu$_4$ and **8**-Tb$_4$ displayed measurable emission spectra. The excitation and emission spectra are displayed in Figures S28 and 8. Both excitation spectra show broad bands with a maximum at around 350 nm, indicating the ligand-centred transitions of tfa, hfa and phen. For **6**-Eu$_4$, the two strong narrow lines at 395 nm ($^5L_6 \leftarrow {}^7F_0$) and 465 nm ($^5D_2 \leftarrow {}^7F_0$) are characteristic of direct excitation of the Eu^{III} ion.[30] For **8**-Tb$_4$, the direct excitation peak is located at 485 nm ($^5D_4 \leftarrow {}^7F_6$).[31]
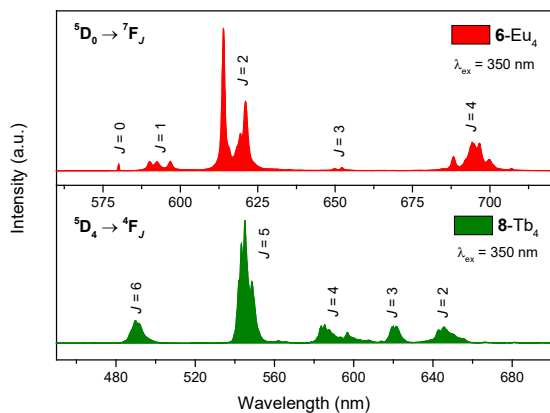
Figure 8. The emission spectra of **6**-Eu$_4$ and **8**-Tb$_4$ at room temperature. Measurement condition: λ_{ex} = 350 nm, slit = 2.0–0.5 nm, longpass filter = 420 nm.

The emission spectrum of **6**-Eu$_4$ is assigned to $^5D_0 \rightarrow {}^7F_J$ (J = 0–4) transitions under excitation at 350 nm. The asymmetric ratio (the intensity ratio of the transitions J = 2 and J = 1) of **6**-Eu$_4$ is 7.58; the large value is attributed to the low symmetry of the Eu^{III} centre, and this is in agreement with the crystal structure.[32] The single peak at 580 nm ($^5D_0 \rightarrow {}^7F_0$ transition) indicates only one type of coordination environment for the Eu^{III} ions in the complex.[32] The luminescence decay profile of $^5D_0 \rightarrow {}^7F_2$ transition was fitted with a monoexponential decay, indicating the presence of a single emitting species in the **6**-Eu$_4$ sample, and the resulting lifetime is 674 μs (Figure S29).

In the case of **8**-Tb$_4$, the emission spectrum shows characteristic $^5D_4 \rightarrow {}^7F_J$ (J = 6–2) transition. The intensity ratio of the $^5D_4 \rightarrow {}^7F_5$ and $^5D_4 \rightarrow {}^7F_6$ transitions is 4.17, suggesting a low symmetry of Tb^{III} ion site – the same situation as in the isostructural **6**-Eu$_4$. The luminescence decay lifetime of the $^5D_4 \rightarrow {}^7F_5$ transition is also monoexponential and determined to be 90 μs (Figure S29). The shorter luminescence lifetime of **8**-Tb$_4$ than **6**-Eu$_4$ is due to the Tb^{III} ion having experienced a more effective non-radiative quenching *via* OH oscillator.

An energy level diagram can be constructed by using the triplet energies of the ligands (Figure 9). The literature values are 22000 cm^{-1} (hfa), 23000 cm^{-1} (tfa) and 22100 cm^{-1} (phen).[33] The phosphorescence spectrum of **1**-La$_4$ was also measured at 20 K (Figure S30) with the domination of the hfa triplet at 459 nm (21800 cm^{-1}). The energy gaps between hfa triplet and $^5D_1$ excited state of the Eu^{III} ion were determined to be 2600 cm^{-1}, which allows efficient energy transfer. However, the triplet of hfa and phen is close to the $^5D_4$ state of the Tb^{III} ion and therefore efficient sensitization is only caused by tfa with the energy gap of 2500 cm^{-1}. This explains that without tfa, **10**-Tb$_2$ has an inefficient sensitization and weak luminescence at room temperature results.
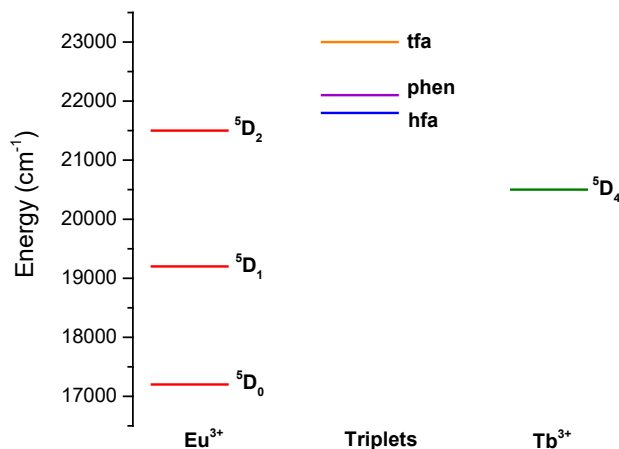

Figure 9. Energy level diagram of the excited state of Eu^{III} and Tb^{III} ion and the triplet state of ligands.

Besides, the O–H oscillating phonons can quench **10**-Tb$_2$ emission non-radiatively.[16] The IR spectrum in Figure 2 determines that the vibrational energies of the bridging O–H of **8**-Tb$_4$ (μ_3-OH) and **10**-Tb$_2$ (μ-OH) are 3619 and 3693 cm^{-1}, respectively. While the free Tb^{III} energy gap is 14800 cm^{-1}, four vibrational quanta of μ_3-OH (~14800 cm^{-1}) bond can deactivate Tb^{III}

luminescence more efficiently than those of the μ-OH (~14500 cm^{-1}) bond. This stronger deactivation accounts for why **10**-Tb$_2$ is weakly luminescent compared with **8**-Tb$_4$.

Since oscillation is suppressed and back energy transfer from first excited state to triplet state is reduced at low temperature, **10**-Tb$_2$ displays characteristic Tb^{III} transition with a lifetime ($^5D_4 \rightarrow$ $^7F_5$) of 854 μs (Figure S31). High resolution spectra of **6**-Eu$_4$ and **8**-Tb$_4$ at 20 K were also recorded, and they revealed the C$_1$ symmetry of the cubane clusters (Figures S32 and S33). Furthermore, their lifetime become longer with the values of 763 μs for **6**-Eu$_4$ and 1505 μs for **8**-Tb$_4$ (Figures S32 and S33). A more than 10-fold increase in lifetime is observed for **8**-Tb$_4$, implying that the O–H bond oscillation quenches Tb^{III} more efficiently than Eu^{III}.

CONCLUSION

This work highlighted the synthesis and characterization of a series of lanthanide(III) hydroxo clusters with tetranuclear cubane-like and dinuclear cores. The assembly was accomplished by the use of β-diketones, carboxylic acids and phenanthroline. The magnetic and photophysical properties were studied. Compounds **8**-Tb$_4$, **9**-Dy$_4$ and **11**-Dy$_2$, ferromagnetically coupled, exhibit SMM behaviour and the Dy^{III} clusters show measurable anisotropic barriers (67.0 K, 82.5 K for **9**-Dy$_4$ and **11**-Dy$_2$ respectively). Compounds **6**-Eu$_4$ and **8**-Tb$_4$ display characteristic red and green emission under photoexcitation at room temperature while **10**-Tb$_2$ is luminescent at 20 K. Work on developing other functional polynuclear compounds is being undertaken.

EXPERIMENTAL SECTION

General considerations. All chemicals used for synthesis were obtained from Sigma-Aldrich and Acros Organics and used without further purification. Elemental analysis was performed by using

an Elementar Vario Micro Cube elemental analyzer. FT-IR spectra were recorded by using the Nicolet™ iS™ 50 FT-IR Spectrometer with KBr pellet.

Crystallographic data. A suitable crystal was picked and mounted using the "oil-drop mounting" technique,[34] and its data were collected using either the Bruker Smart Apex II or Bruker D8-Venture single crystal diffractometer. Multi-scan absorption correction was then applied to the data using the Bruker SAINT/SADABS software.[35,36] The SHELX program suite[37] was used to calculate the initial structural solution through either direct or Patterson method, and then be refined by full matrix least-squares on F2.

Magnetic measurement. Magnetic susceptibility measurements were obtained by using a Quantum Design MPMS-XL7 SQUID magnetometer and a Quantum Design PPMS-XL9 VSM. AC susceptibility data were collected with a 5 Oe switching field at frequencies between 1 and 1488 Hz. Data correction for diamagnetic contribution was calculated from Pascal constants.

Photoluminescence measurement. Steady-state room temperature solid-state photoluminescence measurements were performed with a PTI QuantaMaster™ 50 spectrophotometer equipped with a 75 W xenon arc lamp, double emission monochromator using 400 nm blazed 1200 lines per mm and a Hamamatsu R928 PMT thermoelectrically cooled. Solid sample was prepared by crushing the crystal and the powder was clipped between two quartz plates, held by a rotatable sample holder which oriented at 30º. Low temperature measurements were achieved by using the Advanced Research System (ARS) DE-202 Cryocooler connected with the water-cooled ARS-2HW compressor that circulated helium. The sample was clipped between two quartz plates and held in the cryocooler. The luminescence decay lifetimes were recorded by using the PTI GL-3300

Nitrogen Laser delivering a pulse at 337 nm. The monoexponential curve was fitted using OriginPro.

Synthesis of clusters. *La$_4$(μ_3-OH)$_4$(μ-tfa)$_4$(hfa)$_4$(phen)$_4$ (1-La$_4$)*. To a mixture of trifluoroacetic acid (0.11 g, 1 mmol), hexafluoroacetylacetone (0.42 g, 2 mmol) and 1,10-phenanthroline (0.18 g, 1 mmol) in ethanol (5 mL) in a vial at 60°C, freshly prepared 1 M NaOH solution (3.5 mL) was added, resulting in a yellow solution. The mixture was heated and stirred for 20 minutes. Addition of aqueous solution (1 mL) of lanthanum(III) chloride heptahydrate (0.37 g, 1 mmol) followed. A white solid was formed immediately and the mixture was heated for 3 hours. The solid was then filtered, washed with water and petroleum ether, and recrystallized with the mixture of acetone and ethanol to obtain single crystals. The same approach was applied for the Ln^{III} clusters in this study. Yield: 60% (based on the La^{III} salt). ^{1}H NMR (400 MHz, DMSO-d^6) δ 5.60 (s, 4H), δ 7.79 (m, 8H), δ 8.01 (m, 8H), δ 8.51 (m, 8H), δ 9.12 (m, 8H). Elemental analysis (%) calcd for C$_{76}$H$_{40}$N$_8$O$_{20}$F$_{36}$La$_4$: C, 34.78; H, 1.54; N, 4.27, found: C, 34.25; H, 1.58; N, 4.31. IR (KBr, cm^{-1}): 3597 (m, υ(O-H)), 1686 (s, υ(C=O)), 1497 (s, υ(C=N)), 1255, 1209, 1137, 1103 (s, br, υ(C-F)), 842 (s), 795 (s), 662 (s), 581 (s).

Ce$_4$(μ_3-OH)$_4$(μ-tfa)$_4$(hfa)$_4$(phen)$_4$ (2-Ce$_4$). Yield: 58% (based on the Ce^{III} salt). Elemental analysis (%) calcd for C$_{76}$H$_{40}$N$_8$O$_{20}$F$_{36}$Ce$_4$: C, 34.71; H, 1.53; N, 4.26, found: C, 34.62; H, 1.67; N, 4.25. IR (KBr, cm^{-1}): 3595 (m, υ(O-H)), 1686, 1654 (s, υ(C=O)), 1520 (s, υ(C=N)), 1255, 1205, 1136, 1103 (s, br, υ(C-F)), 843 (s), 796 (s), 662 (s), 581 (s).

Pr$_4$(μ_3-OH)$_4$(μ-tfa)$_4$(hfa)$_4$(phen)$_4$ (3-Pr$_4$). Yield: 67% (based on the Pr^{III} salt). Elemental analysis (%) calcd for C$_{76}$H$_{40}$N$_8$O$_{20}$F$_{36}$Pr$_4$: C, 34.67; H, 1.53; N, 4.26, found: C, 34.52; H, 1.62; N, 4.23. IR

(KBr, cm^{-1}): 3600 (m, υ(O-H)), 1689, 1655 (s, υ(C=O)), 1498 (s, υ(C=N)), 1255, 1206, 1136, 1104 (s, br, υ(C-F)), 842 (s), 795 (s), 663 (s), 584 (s).

Nd$_4$(μ_3-OH)$_4$(μ-tfa)$_4$(hfa)$_4$(phen)$_4$ (4-Nd$_4$). Yield: 57% (based on the Nd^{III} salt). Elemental analysis (%) calcd for C$_{76}$H$_{40}$N$_8$O$_{20}$F$_{36}$Nd$_4$: C, 34.50; H, 1.52; N, 4.23, found: C, 34.58; H, 1.67; N, 4.30. IR (KBr, cm^{-1}): 3605 (m, υ(O-H)), 1691, 1655 (s, υ(C=O)), 1499 (s, υ(C=N)), 1255, 1208, 1135, 1104 (s, br, υ(C-F)), 842 (s), 795 (s), 664 (s), 583 (s).

Sm$_4$(μ_3-OH)$_4$(μ-tfa)$_4$(hfa)$_4$(phen)$_4$ (5-Sm$_4$). Yield: 55% (based on the Sm^{III} salt). Elemental analysis (%) calcd for C$_{76}$H$_{40}$N$_8$O$_{20}$F$_{36}$Sm$_4$: C, 34.18; H, 1.51; N, 4.20, found: C, 33.98; H, 1.62; N, 4.20. IR (KBr, cm^{-1}): 3610 (m, υ(O-H)), 1694, 1655 (s, υ(C=O)), 1501 (s, υ(C=N)), 1255, 1208, 1135, 1104 (s, br, υ(C-F)), 841 (s), 794 (s), 668 (s), 583 (s).

Eu$_4$(μ_3-OH)$_4$(μ-tfa)$_4$(hfa)$_4$(phen)$_4$ (6-Eu$_4$). Yield: 56% (based on the Eu^{III} salt). Elemental analysis (%) calcd for C$_{76}$H$_{40}$N$_8$O$_{20}$F$_{36}$Eu$_4$: C, 34.10; H, 1.51; N, 4.19, found: C, 34.15; H, 1.51; N, 4.19. IR (KBr, cm^{-1}): 3615 (m, υ(O-H)), 1697, 1657 (s, υ(C=O)), 1503 (s, υ(C=N)), 1255, 1205, 1136, 1105 (s, br, υ(C-F)), 842 (s), 794 (s), 669 (s), 583 (s).

Gd$_4$(μ_3-OH)$_4$(μ-tfa)$_4$(hfa)$_4$(phen)$_4$ (7-Gd$_4$). Yield: 59% (based on the Gd^{III} salt). Elemental analysis (%) calcd for C$_{76}$H$_{40}$N$_8$O$_{20}$F$_{36}$Gd$_4$: C, 33.83; H, 1.49; N, 4.15, found: C, 33.82; H, 1.25; N, 4.16. IR (KBr, cm^{-1}): 3620 (m, υ(O-H)), 1698, 1655 (s, υ(C=O)), 1503 (s, υ(C=N)), 1255, 1208, 1135, 1105 (s, br, υ(C-F)), 842 (s), 794 (s), 718 (s), 679 (s), 583 (s).

Tb$_4$(μ_3-OH)$_4$(μ-tfa)$_4$(hfa)$_4$(phen)$_4$ (8-Tb$_4$). Yield: 65% (based on the Tb^{III} salt). Elemental analysis (%) calcd for C$_{76}$H$_{40}$N$_8$O$_{20}$F$_{36}$Tb$_4$: C, 33.75; H, 1.49; N, 4.14, found: C, 33.72; H, 1.54; N, 4.14.

IR (KBr, cm^{-1}): 3620 (m, υ(O-H)), 1698, 1659 (s, υ(C=O)), 1503 (s, υ(C=N)), 1255, 1208, 1136, 1105 (s, br, υ(C-F)), 841 (s), 794 (s), 719 (s), 681 (s), 584 (s).

*Dy$_4$(μ_3-OH)$_4$(μ-tfa)$_4$(hfa)$_4$(phen)$_4$ (**9-Dy$_4$**)*. Yield: 55% (based on the Dy^{III} salt). Elemental analysis (%) calcd for C$_{76}$H$_{40}$N$_8$O$_{20}$F$_{36}$Dy$_4$: C, 33.57; H, 1.48; N, 4.12, found: C, 33.54; H, 1.47; N, 4.10. IR (KBr, cm^{-1}): 3621 (m, υ(O-H)), 1701, 1659 (s, υ(C=O)), 1504 (s, υ(C=N)), 1255, 1208, 1135, 1105 (s, br, υ(C-F)), 841 (s), 794 (s), 719 (s), 685 (s), 584 (s).

*Tb$_2$(μ-OH)$_2$(hfa)$_4$(phen)$_2$ (**10-Tb$_2$**)*. Yield: 63% (based on the Tb^{III} salt). Elemental analysis (%) calcd for C$_{44}$H$_{22}$N$_4$O$_{10}$F$_{24}$Tb$_2$: C, 34.31; H, 1.44; N, 3.64, found: C, 34.30; H, 1.41; N, 3.63. IR (KBr, cm^{-1}): 3694 (m, υ(O-H)), 1659 (s, υ(C=O)), 1507 (s, υ(C=N)), 1258, 1197, 1146, 1099 (s, br, υ(C-F)), 841 (s), 796 (s), 726 (s), 682 (s), 585 (s).

*Dy$_2$(μ-OH)$_2$(hfa)$_4$(phen)$_2$ (**11-Dy$_2$**)*. Yield: 71% (based on the Dy^{III} salt). Elemental analysis (%) calcd for C$_{44}$H$_{22}$N$_4$O$_{10}$F$_{24}$Dy$_2$: C, 34.15; H, 1.43; N, 3.62, found: C, 34.26; H, 1.38; N, 3.62. IR (KBr, cm^{-1}): 3696 (m, υ(O-H)), 1660 (s, υ(C=O)), 1509 (s, υ(C=N)), 1258, 1197, 1146, 1100 (s, br, υ(C-F)), 841 (s), 796 (s), 726 (s), 661 (s), 585 (s).

*Ho$_2$(μ-OH)$_2$(hfa)$_4$(phen)$_2$ (**12-Ho$_2$**)*. Yield: 64% (based on the Ho^{III} salt). Elemental analysis (%) calcd for C$_{44}$H$_{22}$N$_4$O$_{10}$F$_{24}$Ho$_2$: C, 34.04; H, 1.43; N, 3.61, found: C, 35.05; H, 1.35; N, 3.70. IR (KBr, cm^{-1}): 3699 (m, υ(O-H)), 1660 (s, υ(C=O)), 1509 (s, υ(C=N)), 1256, 1198, 1144, 1100 (s, br, υ(C-F)), 841 (s), 796 (s), 726 (s), 661 (s), 585 (s).

*Er$_2$(μ-OH)$_2$(hfa)$_4$(phen)$_2$ (**13-Er$_2$**)*. Yield: 63% (based on Er^{III} salt). Elemental analysis (%) calcd for C$_{44}$H$_{22}$N$_4$O$_{10}$F$_{24}$Er$_2$: C, 33.94; H, 1.42; N, 3.60, found: C, 34.00; H, 1.28; N, 3.58. IR (KBr, cm^{-}

^{1}): 3700 (m, υ(O-H)), 1660 (s, υ(C=O)), 1510 (s, υ(C=N)), 1258, 1197, 1143, 1101 (s, br, υ(C-F)), 841 (s), 796 (s), 726 (s), 661 (s), 586 (s).

Tm$_2$(μ-OH)$_2$(hfa)$_4$(phen)$_2$ (14-Tm$_2$). Yield: 64% (based on the Tm^{III} salt). Elemental analysis (%) calcd for C$_{44}$H$_{22}$N$_4$O$_{10}$F$_{24}$Tm$_2$: C, 33.87; H, 1.42; N, 3.59, found: C, 33.88; H, 1.48; N, 3.55. IR (KBr, cm^{-1}): 3702 (m, υ(O-H)), 1661 (s, υ(C=O)), 1510 (s, υ(C=N)), 1258, 1198, 1143, 1101 (s, br, υ(C-F)), 841 (s), 796 (s), 662 (s), 586 (s).

Yb$_2$(μ-OH)$_2$(hfa)$_4$(phen)$_2$ (15-Yb$_2$). Yield: 69% (based on the Yb^{III} salt). Elemental analysis (%) calcd for C$_{44}$H$_{22}$N$_4$O$_{10}$F$_{24}$Yb$_2$: C, 33.69; H, 1.41; N, 3.57, found: C, 33.73; H, 1.24; N, 3.57. IR (KBr, cm^{-1}): 3704 (m, υ(O-H)), 1663 (s, υ(C=O)), 1511 (s, υ(C=N)), 1258, 1197, 1139, 1101 (s, br, υ(C-F)), 841 (s), 796 (s), 662 (s), 586 (s).

Lu$_2$(μ-OH)$_2$(hfa)$_4$(phen)$_2$ (16-Lu$_2$). Yield: 51% (based on Lu^{III} salt). Elemental analysis (%) calcd for C$_{44}$H$_{22}$N$_4$O$_{10}$F$_{24}$Lu$_2$: C, 33.61; H, 1.41; N, 3.56, found: C, 33.99; H, 1.15; N, 3.58. IR (KBr, cm^{-1}): 3707 (m, υ(O-H)), 1663 (s, υ(C=O)), 1511 (s, υ(C=N)), 1258, 1198, 1144, 1102 (s, br, υ(C-F)), 841 (s), 796 (s), 662 (s), 587 (s).

ASSOCIATED CONTENT

Supporting **Information**

The following files are available free of charge.
^{1}H NMR spectra, FT-IR spectra, crystal structures, luminescent and magnetic data (PDF)
X-ray Crystallographic data for **1**-La$_4$, **2**-Ce$_4$, **2**-Ce$_4$-150K, **3**-Pr$_4$, **4**-Nd$_4$, **5**-Sm$_4$, **6**-Eu$_4$, **7**-Gd$_4$, **8**-Tb$_4$, **9**-Dy$_4$, **10**-Tb$_2$, **11**-Dy$_2$, **12**-Ho$_2$, **13**-Er$_2$, **14**-Tm$_2$,**15**-Yb$_2$, **16**-Lu$_2$ (CCDC 1553239, 1553240,

1553241, 1553242, 1460825, 1553243, 1553244, 1553245, 1553246, 1553247, 1553525, 1553524, 1553248, 1553249, 1553250, 1460824, 1553251) (CIF)

AUTHOR INFORMATION

Corresponding Author

*Email: ga-lai.law@polyu.edu.hk

Author Contributions

The manuscript was written through contributions of all authors. All authors have given approval to the final version of the manuscript.

ACKNOWLEDGMENT

REFERENCES

1. Wagner, A. T.; Roesky, P. W., Rare-Earth Metal Oxo/Hydroxo Clusters – Synthesis, Structures, and Applications. *Eur. J. Inorg. Chem.* **2016**, *6*, 782–791.

2. Andrews, P. C.; Gee, W. J.; Junk, P. C.; Massi, M., Variation of Structural Motifs in Lanthanoid Hydroxo Clusters by Ligand Modification. *New J. Chem.* **2013**, *37*, 35–48.

3. (a) Andrews, P. C.; Beck, T.; Fraser, B. H.; Junk, P. C.; Massi, M.; Moubaraki, B.; Murray, K. S.; Silberstein, M., Functionalised β-Diketonate Polynuclear Lanthanoid Hydroxo Clusters: Synthesis, Characterisation, and Magnetic Properties. *Polyhedron* **2009**, *28*, 2123–2130. (b) Andrews, P. C.; Beck, T.; Forsyth, C. M.; Fraser, B. H.; Junk, P. C.; Massi, M.; Roesky, P. W., Templated Assembly of a μ_6-CO_3^{2-} Dodecanuclear Lanthanum Dibenzoylmethanide Hydroxido Cluster with Concomitant Formation of Phenylglyoxylate. *Dalton Trans.* **2007**, 5651–5654.

4. (a) Li, X.-L.; Li, F.-C.; Zhang, X.-L.; Liu, Y.-F.; Wang, A.-L.; Tian, J.-F.; Xiao, H.-P., Synthesis, Crystal Structures and Magnetic Properties of Two Tetranuclear Lanthanide-Hydroxo Cubane Clusters. *Synth. Met.* **2015**, *209*, 220–224. (b) Gao, H. L.; Jiang, L.; Liu, S.; Shen, H. Y.; Wang, W. M.; Cui, J. Z., Multiple Magnetic Relaxation Processes, Magnetocaloric Effect and Fluorescence Properties of Rhombus-Shaped Tetranuclear Rare Earth Complexes. *Dalton Trans.* **2016**, *45*, 253–264.

5. Zheng, Z., Ligand-Controlled Self-Assembly of Polynuclear Lanthanide–Oxo/Hydroxo Complexes: From Synthetic Serendipity to Rational Supramolecular Design. *Chem. Commun.* **2001**, 2521–2529.

6. Groom, C. R.; Allen, F. H., The Cambridge Structural Database in Retrospect and Prospect. *Angew. Chem. Int. Ed.* **2014**, *53*, 662–671.

7. (a) Freedman, D.; Melman, J. H.; Emge, T. J.; Brennan, J. G., Cubane Clusters Containing Lanthanide Ions: $(py)_8Yb_4Se_4(SePh)_4$ and $(py)_{10}Yb_6S_6(SPh)_6$. *Inorg. Chem.* **1998**, *37*, 4162–4163. (b) Freedman, D.; Sayan, S.; Emge, T. J.; Croft, M.; Brennan, J. G., Heterovalent Clusters: $Ln_4Se(SePh)_8(Ln_4= Sm_4, Yb_4, Sm_2Yb_2, Nd_2Yb_2)$. *J. Am. Chem. Soc.* **1999**, *121*, 11713–11719.

8. Woodruff, D. N.; Winpenny, R. E.; Layfield, R. A., Lanthanide Single-Molecule Magnets. *Chem. Rev.* **2013**, *113*, 5110–5148.

9. Ding, Y.-S.; Chilton, N. F.; Winpenny, R. E. P.; Zheng, Y.-Z., On Approaching the Limit of Molecular Magnetic Anisotropy: A Near-Perfect Pentagonal Bipyramidal Dysprosium(III) Single-Molecule Magnet. *Angew. Chem. Int. Ed.* **2016**, *55*, 16071–16074.

10. Goodwin, C. A. P.; Ortu, F.; Reta, D.; Chilton, N. F.; Mills, D. P., Molecular Magnetic Hysteresis at 60 Kelvin in Dysprosocenium. *Nature* **2017**, *548*, 439–442.

11. Zhang, P.; Guo, Y.-N.; Tang, J., Recent Advances in Dysprosium-Based Single Molecule Magnets: Structural Overview and Synthetic Strategies. *Coord. Chem. Rev.* **2013**, *257*, 1728–1763.

12. Blagg, R. J.; Muryn, C. A.; McInnes, E. J.; Tuna, F.; Winpenny, R. E., Single Pyramid Magnets: Dy_5 Pyramids with Slow Magnetic Relaxation to 40 K. *Angew. Chem. Int. Ed.* **2011**, *50*, 6530–6533.

13. Liu, K.; Zhang, X.; Meng, X.; Shi, W.; Cheng, P.; Powell, A. K., Constraining the Coordination Geometries of Lanthanide Centers and Magnetic Building Blocks in Frameworks: A New Strategy for Molecular Nanomagnets. *Chem. Soc. Rev.* **2016**, *45*, 2423–2439.

14. Eliseeva, S. V.; Bünzli, J.-C. G., Lanthanide Luminescence for Functional Materials and Bio-Sciences. *Chem. Soc. Rev.* **2010**, *39*, 189–227.

15. (a) Moore, E. G.; Samuel, A. P. S.; Raymond, K. N., From Antenna to Assay: Lessons Learned in Lanthanide Luminescence. *Acc. Chem. Res.* **2009**, *42*, 542–552. (b) Lo, W.-S.; Zhang, J.; Wong, W.-T.; Law, G.-L., Highly Luminescent Sm^{III} Complexes with Intraligand Charge-Transfer Sensitization and the Effect of Solvent Polarity on Their Luminescent Properties. *Inorg. Chem.* **2015**, *54*, 3725–3727. (c) Dai, L.; Lo, W. S.; Coates, I. D.; Pal, R.; Law, G. L., New Class of Bright and Highly Stable Chiral Cyclen Europium Complexes for Circularly Polarized Luminescence Applications. *Inorg. Chem.* **2016**, *55*, 9065–9070.

16. Eliseeva, S. V.; Bünzli, J.-C. G. Basics of Lanthanide Photophysics. in *Springer Series on Fluorescence: Lanthanide Luminescence: Photophysical, Analytical and Biological Aspects*; Wolfbeis, O. S., Hof, M.; Springer Verlag: Berlin, **2011**; Vol. 7, Chapter 1, pp 1–45.

17. Binnemans, K. Rare-Earth Beta-diketonates. In *Handbook on the Physics and Chemistry of Rare Earths*; Gschneidner, K. A., Jr., Bünzli, J.-C. G, Pecharsky, V. K.; Elsevier Science B V: Amsterdam, **2005**; Vol. 35, Chapter 225, pp 107–269.

18. (a) Petit, S.; Baril-Robert, F.; Pilet, G.; Reber, C.; Luneau, D., Luminescence Spectroscopy of Europium(III) and Terbium(III) Penta-, Octa- and Nonanuclear Clusters With β-

Diketonate Ligands. *Dalton Trans.* **2009**, 6809–6815. (b) Chen, X. Y.; Yang, X.; Holliday, B. J., Metal-Controlled Assembly of Near-Infrared-Emitting Pentanuclear Lanthanide β-Diketone Clusters. *Inorg. Chem.* **2010**, *49*, 2583–2585. (c) Thielemann, D. T.; Wagner, A. T.; Rosch, E.; Kolmel, D. K.; Heck, J. G.; Rudat, B.; Neumaier, M.; Feldmann, C.; Schepers, U.; Brase, S.; Roesky, P. W., Luminescent Cell-Penetrating Pentadecanuclear Lanthanide Clusters. *J. Am. Chem. Soc.* **2013**, *135*, 7454–7457. (d) Li, X.-L.; Zhu, C.; Zhang, X.-L.; Hu, M.; Wang, A.-L.; Xiao, H.-P., Two Lanthanide-Hydroxo Clusters with Different Nuclearity: Synthesis, Structures, Luminescent and Magnetic Properties. *J. Mol. Struct.* **2017**, *1128*, 30–35.

19. Plakatouras, J. C.; Baxter, I.; Hursthouse, M. B.; Malik, K. M. A.; McAleese, J.; Drake, S. R., Synthesis and Structural Characterisation of Two Novel Gd[III] β-Diketonates [Gd$_4$(μ$_3$-OH)$_4$(μ$_2$-H$_2$O)$_2$(H$_2$O)$_4$(hfpd)$_8$]·2C$_6$H$_6$·H$_2$O and [Gd(hfpd)$_3$(Me$_2$CO)(H$_2$O)] (hfpd-H = 1,1,1,5,5,5-hexafluoropentane-2,4-dione). *J. Chem. Soc., Chem. Commun.* **1994**, 2455–2456.

20. Johnson, D. A.; Waugh, A. B.; Hambley, T. W.; Taylor, J. C., Synthesis and Crystal Structure of 1,1,1,5,5,5-Hexafluoro-2-aminopentan-4-one (HFAP). *J. Fluorine Chem.* **1985**, *27*, 371-378.

21. Tong, Y.-Z.; Wang, Q.-L.; Yang, G.; Yang, G.-M.; Yan, S.-P.; Liao, D.-Z.; Cheng, P., Hydrolytic Synthesis and Structural Characterization of Five Hexanuclear Oxo-Hydroxo Lanthanide Clusters. *CrystEngComm* **2010**, *12*, 543–548.

22. (a) Wu, Y.; Morton, S.; Kong, X.; Nichol, G. S.; Zheng, Z., Hydrolytic Synthesis and Structural Characterization of Lanthanide-Acetylacetonato/Hydroxo Cluster Complexes−A

Systematic Study. *Dalton Trans.* **2011**, *40*, 1041–1046. (b) Hutchings, A.-J.; Habib, F.; Holmberg, R. J.; Korobkov, I.; Murugesu, M., Structural Rearrangement Through Lanthanide Contraction in Dinuclear Complexes. *Inorg. Chem.* **2014**, *53*, 2102–2112.

23. (a) Xu, J.; Radkov, E.; Ziegler, M.; Raymond, K. N., Plutonium(IV) Sequestration: Structural and Thermodynamic Evaluation of the Extraordinarily Stable Cerium(IV) Hydroxypyridinonate Complexes. *Inorg. Chem.* **2000**, *39*, 4156–4164. (b) Daumann, L. J.; Tatum, D. S.; Andolina, C. M.; Pacold, J. I.; D'Aléo, A.; Law, G.-L.; Xu, J.; Raymond, K. N., Effects of Ligand Geometry on the Photophysical Properties of Photoluminescent Eu(III) and Sm(III) 1-Hydroxypyridin-2-one Complexes in Aqueous Solution. *Inorg. Chem.* **2016**, *55*, 114–124.

24. Zhang, J.; Zhang, H.; Chen, Y.; Zhang, X.; Li, Y.; Liu, W.; Dong, Y., A Series of Dinuclear Lanthanide Complexes with Slow Magnetic Relaxation for Dy_2 and Ho_2. *Dalton Trans.* **2016**, *45*, 16463–16470.

25. Wang, Y.; Li, X. L.; Wang, T. W.; Song, Y.; You, X. Z., Slow Relaxation Processes and Single-Ion Magnetic Behaviors in Dysprosium-Containing Complexes. *Inorg. Chem.* **2010**, *49*, 969–976.

26. Xu, G. F.; Wang, Q. L.; Gamez, P.; Ma, Y.; Clerac, R.; Tang, J.; Yan, S. P.; Cheng, P.; Liao, D. Z., A Promising New Route Towards Single-Molecule Magnets Based on the Oxalate Ligand. *Chem. Commun.* **2010**, *46*, 1506–1508.

27. (a) Das, S.; Dey, A.; Biswas, S.; Colacio, E.; Chandrasekhar, V., Hydroxide-Free Cubane-Shaped Tetranuclear $[Ln_4]$ Complexes. *Inorg. Chem.* **2014**, *53*, 3417–3426. (b) Peng, J.-B.;

Ren, Y.-P.; Kong, X.-J.; Long, L.-S.; Huang, R.-B.; Zheng, L.-S., A Series of Di-, Tri- and Tetranuclear Lanthanide Clusters with Slow Magnetic Relaxation for Dy_2 and Dy_4. *CrystEngComm* **2011**, *13*, 2084–2090. (c) Savard, D.; Lin, P. H.; Burchell, T. J.; Korobkov, I.; Wernsdorfer, W.; Clerac, R.; Murugesu, M., Two-dimensional Networks of Lanthanide Cubane-Shaped Dumbbells. *Inorg. Chem.* **2009**, *48*, 11748–11754. (d) Gao, Y.; Xu, G. F.; Zhao, L.; Tang, J.; Liu, Z., Observation of Slow Magnetic Relaxation in Discrete Dysprosium Cubane. *Inorg. Chem.* **2009**, *48*, 11495–11497 (e) Yi, X.; Bernot, K.; Calvez, G.; Daiguebonne, C.; Guillou, O., 3D Organization of Dysprosium Cubanes. *Eur. J. Inorg. Chem.* **2013**, 5879–5885. (f) Ke, H.; Gamez, P.; Zhao, L.; Xu, G. F.; Xue, S.; Tang, J., Magnetic Properties of Dysprosium Cubanes Dictated by the M–O–M Angles of the $[Dy_4(\mu_3\text{-}OH)_4]$ Core. *Inorg. Chem.* **2010**, *49*, 7549–7557. (g) Yao, R.-X.; Xu, X.; Zhang, X.-M., Ferromagnetically Coupled Chiral Dysprosium Hydroxysulfate and Centrosymmetric Dysprosium Hydroxysulfate-Oxalate: $Dy_4(OH)_4$ Cubane Based High-Connected Networks *via in situ* Conversion of Organosulfur to Sulfate. *RSC Adv.* **2014**, *4*, 53954–53959. (h) Ma, B.-Q.; Zhang, D.-S.; Gao, S.; Jin, T.-Z.; Yan, C.-H.; Xu, G.-X., From Cubane to Supercubane: The Design, Synthesis, and Structure of a Three-Dimensional Open Framework Based on a Ln_4O_4 Cluster. *Angew. Chem. Int. Ed*. **2000**, *39*, 3644–3646. (i) Gerasko, O. A.; Mainicheva, E. A.; Naumova, M. I.; Neumaier, M.; Kappes, M. M.; Lebedkin, S.; Fenske, D.; Fedin, V. P., Sandwich-Type Tetranuclear Lanthanide Complexes with Cucurbit[6]uril: From Molecular Compounds to Coordination Polymers. *Inorg. Chem.* **2008**, *47*, 8869–8880. (j) Andrews, P. C.; Gee, W. J.; Junk, P. C.; MacLellan, J. G., Systematic Study of the Formation of the Lanthanoid Cubane Cluster Motif Mediated by Steric Modification of Diketonate Ligands. *Dalton Trans.* **2011**, *40*, 12169–12179.

28. Li, J.; Han, Y.; Cao, F.; Wei, R. M.; Zhang, Y. Q.; Song, Y., Two Field-Induced Slow Magnetic Relaxation Processes in a Mononuclear Co(II) Complex with a Distorted Octahedral Geometry. *Dalton Trans.* **2016**, *45*, 9279–9284.

29. (a) Gatteschi, D.; Sessoli, R.; Villain, J. *Molecular Nanomagnets*; Oxford University Press: New York, 2006. (b) Zhang, R. X.; Chang, Y. X.; Shen, H. Y.; Wang, W. M.; Zhou, X. P.; Wang, N. N.; Cui, J. Z.; Gao, H. L., Modulation of the Relaxation Dynamics of Linear-Shaped Tetranuclear Rare-Earth Clusters Through Utilizing Different Solvents. *Dalton Trans*. **2016**, *45*, 19117–19126.

30. Carnall, W. T.; Fields, P. R.; Rajnak, K., Electronic Energy Levels of the Trivalent Lanthanide Aquo Ions. IV. Eu^{3+}. *J. Chem. Phys.* **1968**, *49*, 4450–4455.

31. Carnall, W. T.; Fields, P. R.; Rajnak, K., Electronic Energy Levels of the Trivalent Lanthanide Aquo Ions. IV. Tb^{3+}. *J. Chem. Phys.* **1968**, *49*, 4447–4449.

32. Binnemans K. Interpretation of Europium(III) Spectra. *Coord. Chem. Rev.* **2015**, *295*, 1–45.

33. (a) Brito, H. F.; Malta, O. M. L.; Felinto, M. C. F. C.; Teotonio, E. E. S., Luminescence Phenomena Involvng Metal Enolates. In *The Chemistry of Metal Enoates*; Zabicky, J.; Wiley: New York, **2009**; Vol. 1, Chapter 3, pp 132–141. (b) Gropper, H.; Dörr, F., Die Orientierung der optischen Übergangsmomente in Phenanthren und seinen Azaderivaten. *Ber. Bunsen-Ges. Phys. Chem.* **1963**, *67*, 46–54.

34. SAINT; Bruker AXS Inc., Madison, Wisconsin, USA, 2007.

35. SAINT; Bruker AXS Inc., Madison, Wisconsin, USA, 2012.

36. SADABS; Bruker AXS Inc., Madison, Wisconsin, USA, 2001.

37. Sheldrick, G. M., A short history of SHELX. *Acta Cryst.* **2008**, *A64*, 112–122.

For Table of Contents Only
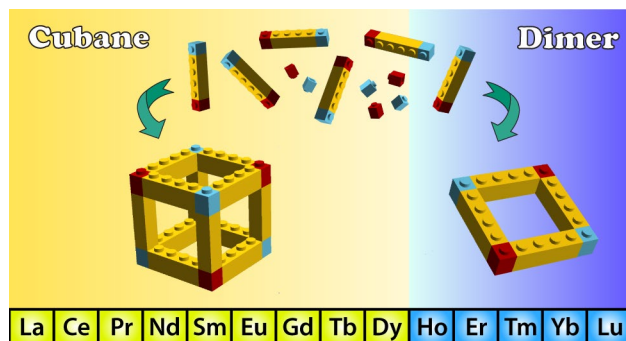
SYNOPSIS. Two types of lanthanide(III) compounds, namely hydroxo cubane-like tetranuclear and dinuclear clusters, were synthesized and characterized. Extensive π-stacking arrays by phenanthroline were observed in the crystal structures. The Tb^{III} and Dy^{III} cubanes and Dy^{III} dimer were found to be single-molecule magnet. The photoluminescence properties of Eu^{III} and Tb^{III} were studied.